JOURNAL OF MATERIALS SCIENCE 18 (1983) 2163–2172

Crystallization characteristics of amorphous Fe–Si–B alloys

ALICJA ZAŁUSKA, HENRYK MATYJA
Institute of Materials Science and Engineering, Warsaw Technical University, Narbutta 85, 02-524 Warsaw, Poland

Crystallization of soft magnetic Fe–Si–B glasses was investigated by transmission electron microscopy and X-ray diffraction. Electron micrographs of the successive crystallization stages of some Fe–Si–B glasses were obtained and the morphology variations for different alloy compositions were determined. The compositional dependence of the crystallization mode exhibited by the Fe–Si–B glasses was analysed, and on this basis some suggestions about crystallization rules in these glasses are proposed. Two kinds of iron–silicon phases occurred, depending on the Fe–Si–B alloy composition: bcc Fe(Si) solid solution and an ordered solid solution on the structural basis of Fe_3Si iron silicide. It is suggested that the metastable Fe_3B phase (observed during crystallization of only few glasses) was not a simple consequence of boron content. Crystallization of the Fe_3B phase was related to the formation of the iron–silicon phase which was produced during the first crystallization stage.

1. Introduction

Preliminary crystallization studies of ternary Fe–Si–B alloys [1] testified to their very interesting crystallization behaviour. Differences in the relative concentrations of metalloids between these glasses were found to markedly affect the crystallization phases and crystallization temperatures. In some recent works on crystallization of different Fe–Si–B glasses, use has been made of differential scanning calorimetry [2–5], Mössbauer effect [6–14], electron microscopy [15], electrical resistivity [1, 16] and magnetic measurements [17, 18]. Depending on glass compositions (even quite similar ones), different crystallization product structures have been observed, (e.g. $Fe_{82}Si_3B_{15}$ [9]–with Fe_3B phase formation and $Fe_{82}Si_6B_{12}$ [10] or $Fe_{80}Si_4B_{16}$ [6]–without any traces of the Fe_3B phase). Gaining insight into the dependence of the crystallization mode on metalloid contents was the aim of the present paper. Our investigations comprised the following Fe–Si–B glasses: $Fe_{75}Si_6B_{19}$, $Fe_{75}Si_{12}B_{13}$, $Fe_{75}Si_{18}B_7$ and $Fe_{84}Si_6B_{10}$. Transmission electron microscopy and X-ray diffraction were the experimental techniques used.

2. Experimental procedure

Amorphous Fe–Si–B alloys of required compositions were produced using two methods: the melt-spinning technique and the arc-melting technique. Amorphous samples prepared by the arc-melting method were used for the electron microscopic studies because they did not require electrolytic thinning. All X-ray diffraction tests were performed using samples produced by both methods, to make sure that the crystallization processes in these two kinds of samples did not differ. Diffractometric measurements were performed in a Philips PM 8000 diffractometer, using Co$K\alpha$ radiation. Microscopic studies were carried out in a JEM 100B transmission electron microscope operating at accelerating voltage of 100 kV. Amorphous samples were heated in a Perkin-Elmer DSC-2 microcalorimeter to temperatures at which different crystallization stages could be obtained; a heating rate of $10\,K\,min^{-1}$ was used. All investigations were carried out at room temperature.

3. Structure analysis by X-ray diffraction

Generally, alloys with no rapid heat treatment in their thermal history strongly tend to retain the

0022–2461/83 $03.00 + .12

equilibrium phases. Amorphous alloys represent a large departure from the equilibrium state, but can form the equilibrium phases in a subsequent crystallization process. In many cases this does not occur directly, but takes place via formation of different transient metastable phases, (e.g. the Fe_3B phase in crystallization of Fe–B glass). Before characterization of the actual crystallization process in our Fe–Si–B amorphous alloys, it is worthwhile to analyse their phase equilibrium systems. Since unfortunately no ternary Fe–Si–B equilibrium diagram for room temperature is available ([19, 20] presented equilibrium phases at about 1000° C), two of the binary diagrams, Fe–B and Fe–Si, will be considered.

3.1. Fe–B phase equilibrium diagram

This binary system has been mentioned often in recent papers dealing with crystallization of Fe–B amorphous alloys. Fig. 1 shows a fragment of the Fe–B phase equilibrium diagram [21] comprising Fe-rich alloys. It presents only two stable phases at room temperature:

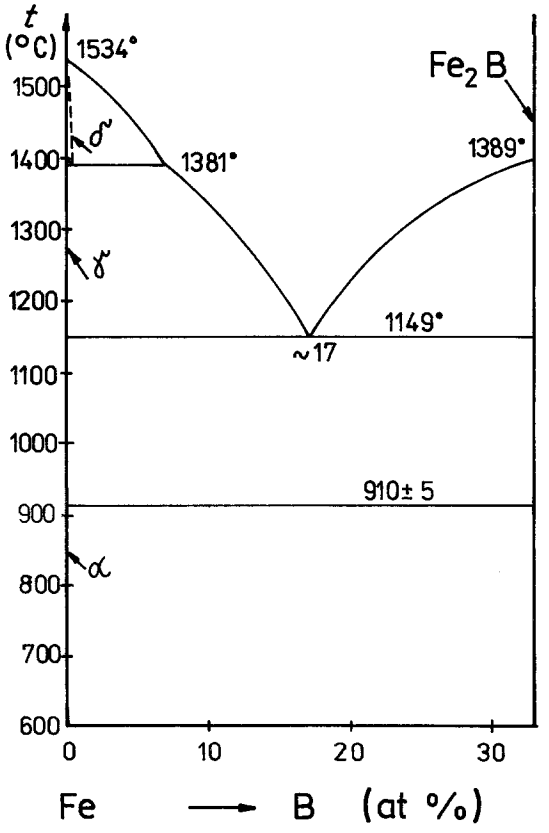

Figure 1 Fe–B phase equilibrium diagram for the region of Fe-rich alloys [21].

1. αFe (bcc structure, lattice parameter $a = 0.286\,64$ nm–ASTM card number 6-0696).

2. Fe_2B (tetragonal structure, lattice parameters: $a = 0.5099$ nm, $c = 0.4240$ nm–ASTM card number 3-1053).

It is noteworthy that both phases are nearly completely immiscible, i.e. boron atoms cannot easily form a solution in the αFe structure and iron boride Fe_2B occurs as a strictly stoichiometric phase. Within the concentration range presented in Fig. 1 (between 0 and 33.3 at% boron) we expect a mixture of two phases: αFe and Fe_2B, as the equilibrium phases at room temperature.

3.2. Fe–Si phase equilibrium diagram

Fig. 2 presents the Fe-rich fragment of the binary Fe–Si equilibrium diagram [22]. The essential difference between the Fe–B and Fe–Si systems lies in the relatively large miscibility regions observed for the phases of the Fe–Si system. For small silicon concentrations, a solid solution α (denoted here as Fe(Si)) occurs. It is a substitutional solution in which silicon atoms occupy the iron sites, with preference for silicon–silicon distances being as large as possible [23]. The second equilibrium phase at room temperature consists of a solid solution α_1 formed on the structural basis of Fe_3Si iron silicide. It is a DO_3-type structure with lattice parameter $a = 0.564$ nm for stoichiometric Fe_3Si (ASTM card number 11-616). The unit cell of this compound consists of eight regular bcc cells (Fig. 3). All corner sites are occupied by iron atoms. At the centre sites, iron and silicon atoms are located alternately. These

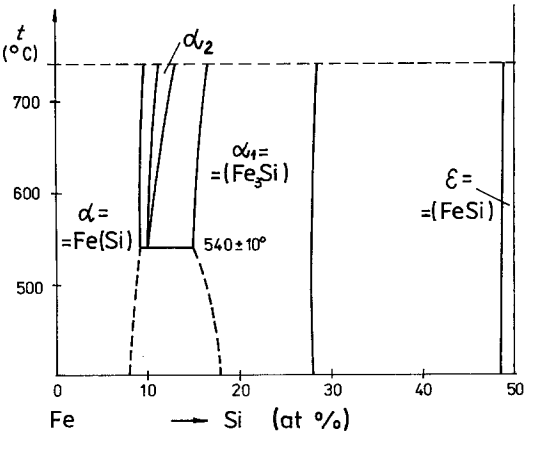

Figure 2 Fe–Si phase equilibrium diagram for the region of Fe-rich alloys [22].

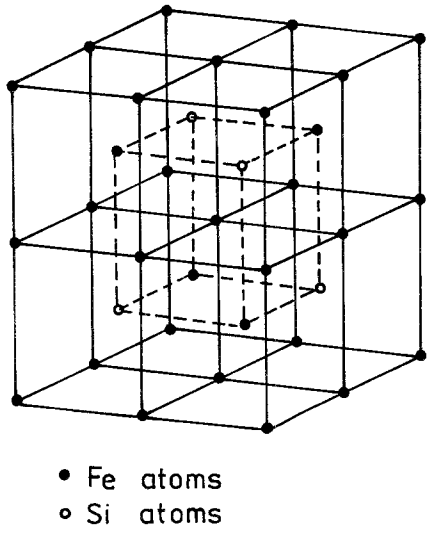

Figure 3 Unit cell of the stoichiometric Fe_3Si phase.

exactly defined silicon sites in the stoichiometric Fe_3Si phase reflect the order of this structure. According to the equilibrium diagram, the Fe_3Si structure exhibits a large miscibility range. This means that the structural nature and kind of atom arrangement are retained also in alloys departing from the stoichiometric concentration $Fe_{75}Si_{25}$. The denotation (Fe_3Si) is used here, in spite of the fact that the phase need not be strictly stoichiometric.

The concentration range limited by dashed lines in Fig. 2 (between ~8 and ~18 at% silicon) is questionable. The phase structure at room temperature within this range has not so far been exactly determined. From the equilibrium diagram, one can expect a eutectoid mixture of the Fe(Si) and (Fe_3Si) phases as a consequence of eutectoid reaction at ~540° C. However, the structural nature of the Fe(Si) and (Fe_3Si) phases makes the differentiation between the random solid solution Fe(Si) and ordered solution (Fe_3Si) very difficult in this concentration range.

3.3. Diffractometric results

X-ray diffraction was used to study crystallization of the amorphous Fe–Si–B alloys investigated. Diffractometric phase analysis showed that the first crystallization stage was always characterized by formation of iron–silicon phases (or, in the $Fe_{75}Si_{12}B_{13}$ alloy, by nearly simultaneous formation of iron–silicon and iron–boron phases). It was observed that the structure of the iron–silicon phase changed for different alloy compositions. Glasses with a low silicon content ($Fe_{84}Si_6B_{10}$ and $Fe_{75}Si_6B_{19}$) exhibited an X-ray diffraction pattern characteristic of the bcc Fe(Si) structure. For alloys with relatively high silicon concentrations ($Fe_{75}Si_{12}B_{13}$, $Fe_{75}Si_{18}B_7$), diffraction peaks characteristic of an ordered (Fe_3Si) structure were observed. Figs. 4a and b exemplify the diffractometric patterns of these two structures. For the $Fe_{75}Si_{18}B_7$ alloy, the extra superlattice reflections of the ordered (Fe_3Si) structure were

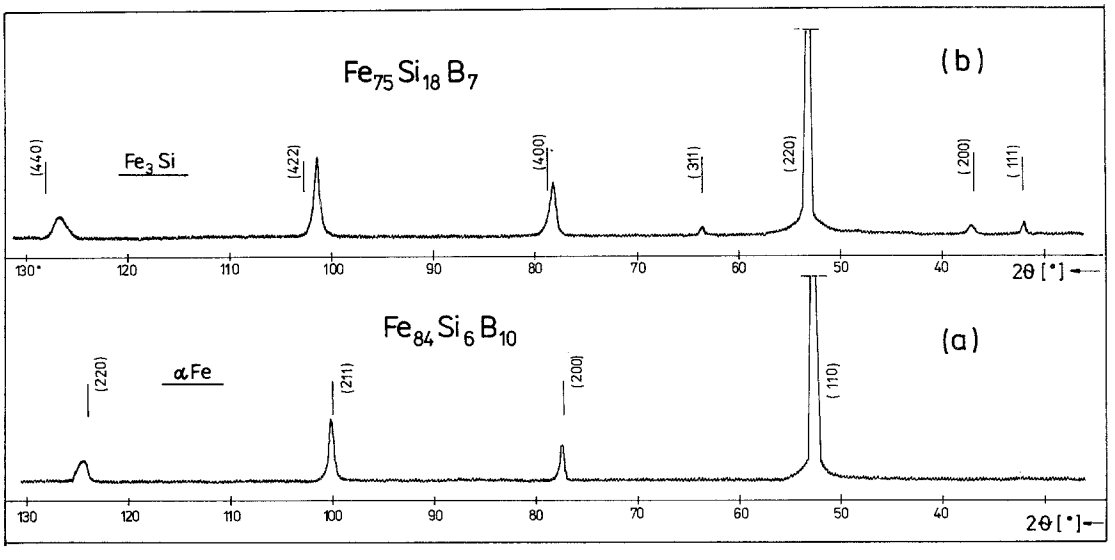

Figure 4 Diffraction patterns of first crystallization stages: (a) glass $Fe_{84}Si_6B_{10}$ annealed to 780 K, and (b) glass $Fe_{75}Si_{18}B_7$ annealed to 790 K. Miller indices and respective 2θ angles for pure αFe and stoichiometric Fe_3Si are taken from ASTM cards.

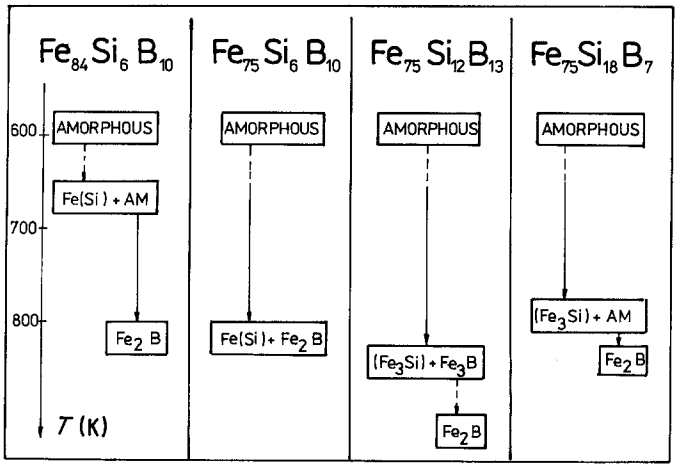

Figure 5 Schematic diagram showing the crystallization stages of the Fe–Si–B glasses investigated.

evident. Of course, both these phases were neither pure αFe nor stoichiometric Fe_3Si, but were solid solutions.

Departure from the stoichiometric compositions caused changes in the lattice parameter. This was reflected in the diffraction patterns as diffraction peak shifts. The Fe(Si) solid solution was characterized by silicon atom substitution in the bcc αFe structure. Silicon atoms are smaller than iron atoms [24]. This induced a decrease in the αFe lattice parameter, (i.e. a decrease in interplanar spacing) and caused diffraction peak shifts to higher 2θ angles (Fig. 4a). In the (Fe_3Si) phase an opposite situation was observed. The (Fe_3Si) solid solution did not attain in the investigated alloys the stoichiometric concentration, i.e. the silicon content was insufficient to form the stoichiometric Fe_3Si structure. In this case some iron atoms were located at the silicon sites in the Fe_3Si structure (Fig. 3). This resulted in an increase in the lattice parameter and in a shift of the diffraction peaks to lower 2θ angles (Fig. 4b). Formation of the Fe(Si) and (Fe_3Si) solutions caused also broadening of the diffraction peaks.

The second crystallization stage of the Fe–Si–B amorphous alloys was characterized by formation of an iron–boron phase. In most of the alloys investigated crystallization of the Fe_2B phase was observed. The $Fe_{75}Si_{12}B_{13}$ glass was an exception; it exhibited formation of transient metastable Fe_3B as an intermediate crystallization stage. Formation of this metastable Fe_3B iron boride has previously been observed for binary Fe–B amorphous alloys [25]. Final crystallization led to the formation of the stable Fe_2B phase, as confirmed by the present results.

These crystallization processes for the Fe–Si–B alloys investigated are presented schematically in Fig. 5.

4. Electron microscope results

In spite of the large interest in crystallization of Fe–Si–B glasses, only few electron micrographs presenting this process have so far been published [26, 27]. Our transmission electron microscope (TEM) observations were designed to illustrate the successive crystallization stages and to determine the morphological changes characteristic of the different crystallizing phases.

Differential scanning calorimetry (DSC) measurements are presented for comparison in Fig. 6 [1].

4.1. $Fe_{75}Si_6B_{19}$ alloy

Calorimetric measurements of the amorphous $Fe_{75}Si_6B_{19}$ alloy (Fig. 6) exhibited only one exothermic crystallization effect. One slim non-diffuse calorimetric peak reflected the relatively high crystallization rate characteristic of this alloy. The rapidity of the crystallization process made observations of the successive crystallization stages very difficult. Fig. 7a shows the beginning of crystallization (formation of the first Fe(Si) crystals), and Fig. 7b presents a fully crystallized sample with cellular microstructure (Fe(Si) + Fe_2B).

4.2. $Fe_{75}Si_{12}B_{13}$ alloy

The thermogram (Fig. 6) of the $Fe_{75}Si_{12}B_{13}$ amorphous alloy shows two distinct exothermic effects. The beginning of the first crystallization stage produced the crystal structure presented in Fig. 8a. Two kinds of crystal were formed nearly simultaneously. The first kind consisted of spheru-

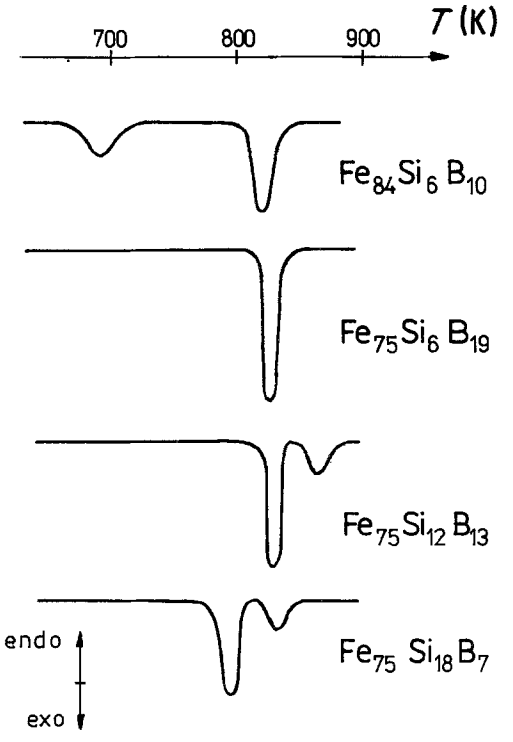

Figure 6 DSC traces taken for glasses heated at a heating rate of 10 K min^{-1}, $dH/dt = 20.9$ mJ sec^{-1}, sample weight = 5 mg.

lites with an intrinsic lamellar microstructure. Their shape was very similar to the Fe_3B crystals formed during crystallization of binary Fe–B amorphous alloys [28]. Electron diffraction analysis indicated that our spherulites also consisted of metastable iron boride Fe_3B (Fig. 8c). Thus, the TEM observations evidently confirmed the X-ray diffraction results indicating that the $Fe_{75}Si_{12}B_{13}$ alloy (as only one of the now investigated Fe–Si–B alloys) crystallizes via metastable iron boride Fe_3B. Crystals of the second kind, formed during the first crystallization stage, were star-shaped or dendritic; they represent the (Fe_3Si) solid solution structure. Fig. 8b presents the continuing crystallization process and Fig. 8d shows the fully crystallized structure, with crystal shapes remaining from the first crystallization stage. The electron diffraction pattern of this structure pointed to the presence of two phases: (Fe_3Si) solid solution and Fe_2B iron boride, with no traces of the decomposed Fe_3B phase.

4.3. $Fe_{75}Si_{18}B_7$ alloy

The $Fe_{75}Si_{18}B_7$ amorphous alloy exhibited two distinct crystallization stages (Fig. 6). TEM studies of this glass confirmed the formation of an ordered (Fe_3Si) solid solution during the first crystallization stage. The complicated dendritic shape of these crystals is shown in Figs. 9a and b. The diffraction pattern obtained for a single dendritic crystal is presented in Fig. 9c. The second phase formed during crystallization consisted of stable iron boride Fe_2B. The microstructure of the fully crystallized alloy is shown in Fig. 9d.

4.4. $Fe_{84}Si_6B_{10}$ alloy

The first crystallization peak obtained in the calorimetric measurement (Fig. 6) could be attributed to the formation of Fe(Si) solid solution. The morphology of crystal formation is shown in Fig. 10a. The second crystallization stage could be enhanced by formation of the Fe_2B phase. The final microstructure of a fully crystallized sample is shown in Fig. 10b.

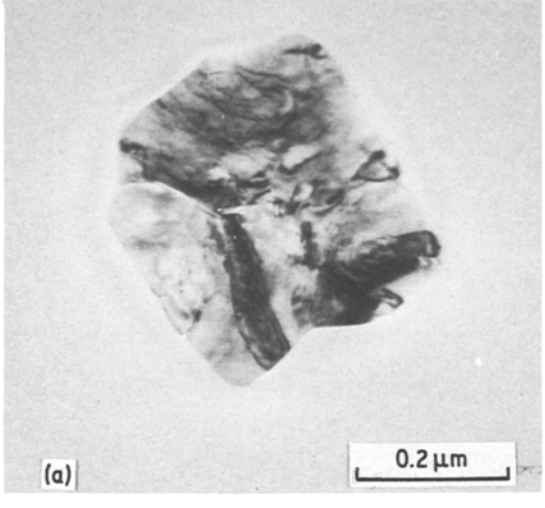

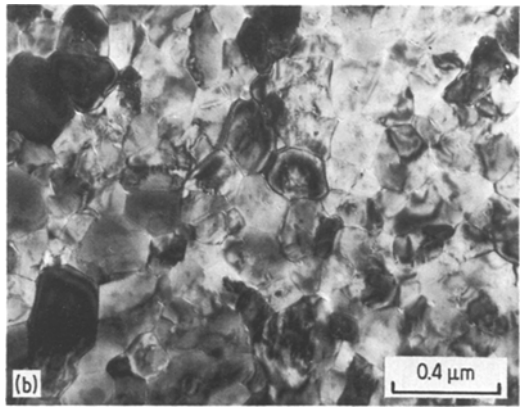

Figure 7 Micrographs of $Fe_{75}Si_6B_{19}$ annealed for 10 min: (a) at 730 K, αFe, and (b) at 800 K, αFe + Fe_2B.

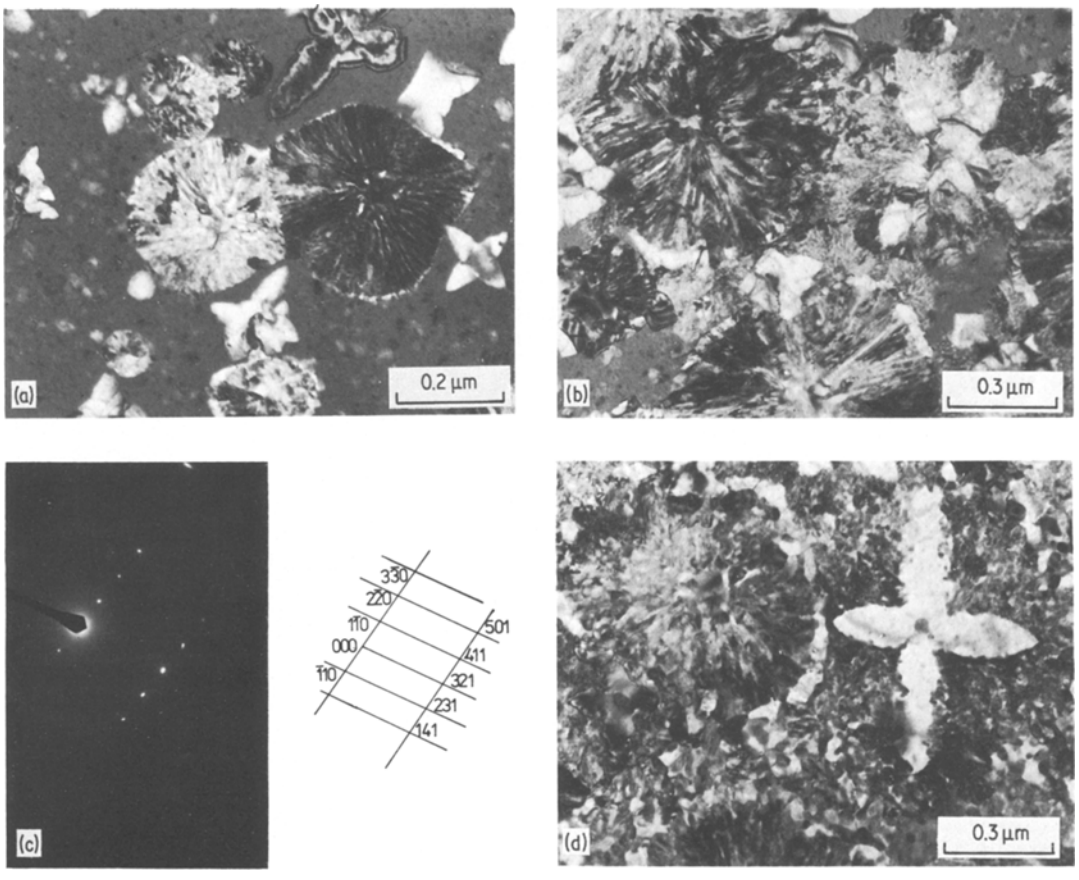

Figure 8 Crystallization of $Fe_{75}Si_{12}B_{13}$ glass: (a) annealing at 775 K for 10 min, $Fe_3Si + Fe_3B$; (b) at 780 K for 10 min, $Fe_3Si + Fe_3B$; (c) diffraction pattern of Fe_3B spherulite; (d) annealing at 820 K for 10 min, $Fe_3Si + Fe_2B$.

5. Discussion and conclusions

The present and earlier X-ray diffraction, electron microscopic and resistivity studies testify to differences in the crystallization processes between different ternary Fe–Si–B amorphous alloys. The phases initially formed were dependent on alloy compositions and, in addition, evident differences in crystallization morphology were found. Metastable iron boride Fe_3B occurred during crystallization of only few glasses: our $Fe_{75}Si_{12}B_{13}$ alloy; $Fe_{80.1}Si_{7.9}B_{12}$, $Fe_{74.8}Si_{15.2}B_{12}$ [2]; $Fe_{84}Si_1B_{15}$, $Fe_{83}Si_2B_{15}$, $Fe_{82}Si_3B_{15}$ [9] and $Fe_{80}Si_2B_{18}$ [6]. Formation of the Fe_3B phase in $Fe_{80.1}Si_{7.9}B_{12}$ glass [2] is doubtful, because it has not been found by other authors [6] in the $Fe_{80}Si_8B_{12}$ alloy. In all remaining glasses only the stable Fe_2B phase was observed. Differences in the structure of the iron–silicon phases were also found. A bcc Fe(Si) solid solution was formed in some alloys while an ordered (Fe_3Si) solid solution appeared in others. Unfortunately, some authors have not differentiated between the random and ordered iron–silicon phases, and stated only that $Fe_{1-z}Si_z$ solutions were formed [9, 10, 13, 18].

It is possible to determine the rules governing the crystallization process, by taking into account only the composition of the alloys investigated. Therefore, we have prepared a diagram presenting the crystallization of the Fe–Si–B alloys investigated so far (our results and data obtained from the literature are listed in Table I). Atom number ratios: Si/Fe and B/Fe, are marked on the horizontal and vertical axes of the diagram, respectively (Fig. 11). Glasses exhibiting formation of the Fe_3B phase are marked by crosses. All remaining alloys, in which crystallization of the Fe_3B phase was not observed, are marked by circles. In order to distinguish between the glasses forming random and ordered Fe–Si solutions, different kinds of circles are used: open circles denote the alloys forming ordered (Fe_3Si) solutions (> 18 at% silicon) and

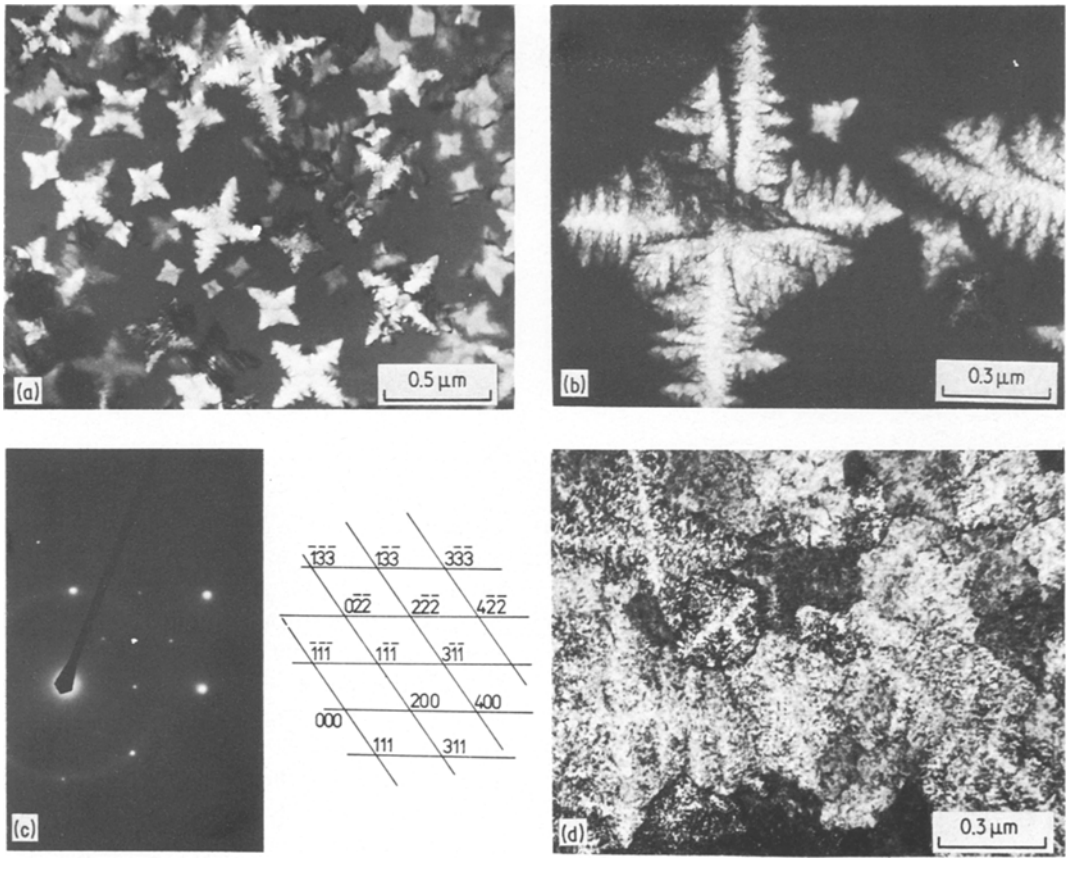

Figure 9 Crystallization of $Fe_{75}Si_{18}B_7$ glass: (a) dendritic crystals Fe_3Si and (b) single dendrite formed during annealing at 740 K for 10 min; (c) diffraction pattern of the crystal presented in Fig. 9b – Fe_3Si structure; (d) fully crystallized microstructure (820 K, 10 min), $Fe_3Si + Fe_2B$.

filled circles represent alloys forming disordered Fe–Si phases. There are also some limiting lines (A, B, C, D) in Fig. 11 which were calculated on the basis of certain assumptions. As can be seen from the diagram, some alloys in which crystallization of the Fe_3B phase occurs, are located in the region characterized by low Si/Fe ratios (shaded region I). This means that for-

TABLE I Compositions of the Fe–Si–B glasses presented in Fig. 11 together with their denotation and reference

Number	Alloy	Reference	Number	Alloy	Reference
1	$Fe_{80}Si_2B_{18}$	[6]	15	$Fe_{80}Si_8B_{12}$	[6]
2	$Fe_{84}Si_1B_{15}$	[9]	16	$Fe_{78}Si_{10}B_{12}$	[26]
3	$Fe_{83}Si_2B_{15}$	[9]	17	$Fe_{84}Si_6B_{10}$	[1, x*]
4	$Fe_{82}Si_3B_{15}$	[8, 9]	18	$Fe_{83}Si_7B_{10}$	[1]
5	$Fe_{75}Si_2B_{23}$	[6]	19	$Fe_{80}Si_{10}B_{10}$	[6]
6	$Fe_{75}Si_4B_{21}$	[6, 7]	20	$Fe_{80}Si_{12}B_8$	[6]
7	$Fe_{75}Si_6B_{19}$	[1, x*]	21	$Fe_{75}Si_{10}B_{15}$	[6, 7, 9]
8	$Fe_{75}Si_9B_{16}$	[7]	22	$Fe_{72.5}Si_{12.5}B_{15}$	[9]
9	$Fe_{76}Si_9B_{15}$	[8]	23	$Fe_{70}Si_{15}B_{15}$	[9]
10	$Fe_{80}Si_3B_{17}$	[6]	24	$Fe_{75}Si_{12}B_{13}$	[1, x*]
11	$Fe_{80}Si_4B_{16}$	[6]	25	$Fe_{74.8}Si_{13.2}B_{12}$	[2]
12	$Fe_{80}Si_5B_{15}$	[9]	26	$Fe_{75}Si_{15}B_{10}$	[1, 7, x*]
13	$Fe_{80}Si_6B_{14}$	[6]	27	$Fe_{75}Si_{18}B_7$	[6, x*]
14	$Fe_{82}Si_6B_{12}$	[10]	28	$Fe_{75}Si_{20}B_5$	[7]

*x – present work.

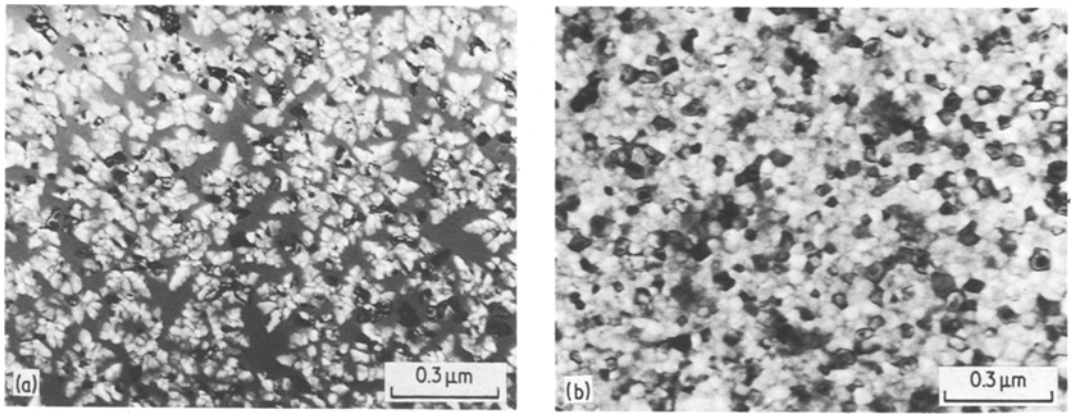

Figure 10 Micrographs of $Fe_{84}Si_6B_{10}$ glass annealed for 10 min: (a) at 660 K, αFe, and (b) at 800 K, αFe + Fe_2B.

mation of the Fe(Si) phase (with low silicon content) was accompanied by crystallization of the Fe_3B phase. In order to evaluate the silicon concentration in the Fe(Si) phase, the number of iron atoms bonded in the Fe_3B phase was subtracted from the total number of iron atoms, resulting from the glass formula. Then the composition of the remaining Fe–Si phase was calculated. According to the Fe–Si phase equilibrium diagram (Fig. 2), the Fe(Si) phase exists as a random solid solution up to a concentration limit of 8 at% silicon. For higher silicon contents, ordering of the Fe–Si phase occurred. Line A in Fig. 11 (calculated on the assumption of the presence of the Fe_3B phase) represents the glass compositions, for which the Fe(Si) phase reaches the limit of existence of a random solution (8 at% silicon). Above that line, ordering processes in the Fe(Si) phase should occur, if the assumption about Fe_3B formation were valid. This is not confirmed by the experimental results. On the other hand, line A seems to be an upper limit of the Fe_3B phase crystallization region at low silicon levels. Thus, the reason why the Fe_3B phase is not observed for the alloy compositions above line A evidently lies in the nature of the Fe(Si) phase. Formation of the Fe_2B phase without metastable phase crystallization leads to bonding of fewer iron atoms in the Fe–B phase, and, as a consequence, the Fe–Si phase should exhibit a lower silicon concentration. Therefore, the necessity of a disordered–ordered transition for alloy compositions above line A in the Fe(Si) phase could be avoided by dispensing with Fe_3B phase formation. Thus, the alloys in that region are characterized by crystallization of the random Fe(Si) phase and Fe_2B phase. From that behaviour a very important conclusion could be drawn: the Fe(Si) phases (crystallizing before the iron–boron phases during continuous heating) are responsible for the absence of Fe_3B formation in this region. Calculations of the silicon concentration in the Fe(Si) phase of these glasses should be done by subtraction of the number of the iron atoms bonded in the Fe_2B phase. An increase in total metalloid

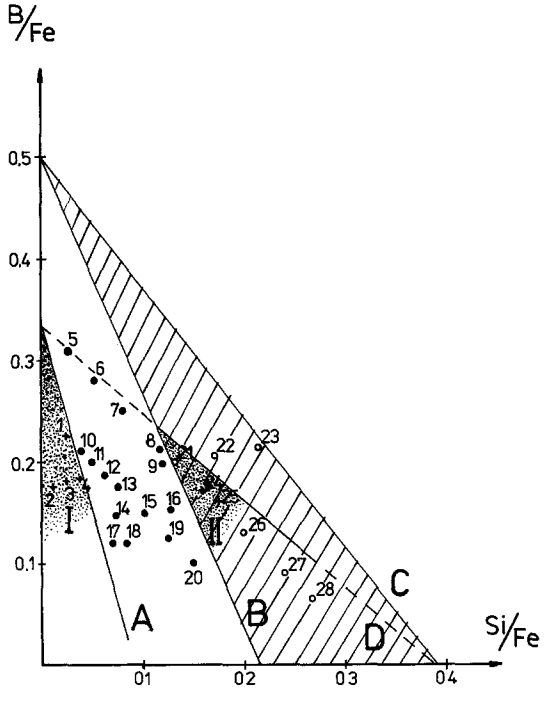

Figure 11 Compositions of glasses in the ternary Fe–Si–B system. Glasses characterized by crystallization of: metastable Fe_3B phase (+), ordered (Fe_3Si) phase (○), and disordered Fe–Si phase (●). Lines A, B, C and D are explained in the text.

contents of the Fe–Si–B glasses considered leads to higher silicon concentrations in the Fe–Si phases. According to the phase equilibrium diagram (Fig. 2), the Fe–Si phases with silicon concentrations higher than 18 at% silicon should exhibit an ordered (Fe_3Si) structure, and the maximum silicon content in this phase is 28 at%. Lines B and C in Fig. 11 represent glass compositions with a constant silicon concentration in the Fe–Si phase (on the assumption that the Fe_2B compound was formed as the Fe–B phase). Line B was calculated for a silicon content of 18 at%. Thus, it should be the limit of a crystalline region – below this line the disordered Fe–Si phase should be formed and above it ordered (Fe_3Si) crystals should occur. This assumption is quite well confirmed by the experimental results (Fig. 11). Line C was calculated for the maximal silicon concentration in the (Fe_3Si) phase, i.e. 28 at% silicon. Above that line the (Fe_3Si) phase should be observed no more. Thus, formation of ordered (Fe_3Si) iron silicide would be expected in the hatched region – between lines B and C. It is of interest that the Fe_3B phase was observed not only below line A in Fig. 11, but also in the second shaded region (II) above line B. This could be explained using the previous conclusion: the Fe–Si phase "allowed" the Fe_3B phase to form in glasses in which this formation requires no changes in the Fe–Si phase structure. This behaviour could be observed also for the alloy compositions for which crystallization of the Fe_3B phase (as well as the Fe_2B phase) permits formation of the same ordered (Fe_3Si) structure. In these alloys formation of metastable Fe_3B occurred. This crystallization region is limited in Fig. 11 by line D. This line was calculated on the assumption of Fe_3B phase formation (like line A) at the characteristic silicon concentration of 28 at%. However, crystallization of the Fe_3B phase was not observed within the whole region between lines B and D. Glasses with relatively high silicon contents (Si/B ratio $\gtrsim 1$) did not exhibit crystallization of the Fe_3B phase and formation of only the (Fe_3Si) and Fe_2B phases was observed.

The crystallization diagram presented in Fig. 11 is thus a simple way of predicting the phases formed in crystallization of ternary amorphous Fe–Si–B alloys. It shows good agreement between the crystallization phases predicted from the diagram and those experimentally observed.

References

1. A. ZAŁUSKA and H. MATYJA, in Proceedings of the Fourth International Conference on Rapidly Quenched Metals, Sendai, Japan, August 1981 edited by T. Masumoto and K. Suzuki, p. 683.
2. K. HOSELITZ, *Phys. Status Solidi (a)* **53** (1979) K23.
3. *Idem, J. Magn. Magn. Mater.* **20** (1980) 201.
4. F. J. A. DEN BROEDER and J. VAN DER BORST, *J. Appl. Phys.* **50** (1979) 4279.
5. M. NAKA, T. MASUMOTO and H. S. CHEN, *J. Physique* **41** (1980) C8-839.
6. U. GONSER, M. GHAFARI, M. ACKERMANN, H. P. KLEIN, J. BAUER and H. -G. WAGNER, in Proceedings of the 4th International Conference on Rapidly Quenched Metals, Sendai, Japan, August 1981 edited by T. Masumoto and K. Suzuki, p. 639.
7. T. KEMÉNY, I. VINCZE, H. A. DAVIES, I. W. DONALD and A. LOVAS, in Proceedings of the 4th International Conference on Metallic Glasses, Budapest, Hungary, June 1980 edited by C. Hargitai, I. Bakonyi and T. Kemény, p. II-239.
8. J. M. DUBOIS, M. BASTICK, G. LE CAER and C. TETE, *Rev. Phys. Appl.* **15** (1980) 1103.
9. S. AL BIJAT, R. IRALDI, C. CUNAT, G. LE CAER, J. M. DUBOIS and C. TETE, in Proceedings of the 4th International Conference on Rapidly Quenched Metals, Sendai, Japan, August 1981 edited by T. Masumoto and K. Suzuki, p. 687.
10. H. N. OK and A. H. MORRISH, *Phys. Rev. B* **22** (1980) 3471.
11. *Idem, ibid. B* **22** (1980) 4215.
12. P. J. SCHURER, A. H. MORRISH and M. J. STAVN, *Phys. Status Solidi (a)* **64** (1981) 343.
13. M. TANIWAKI, M. MAEDA, S. UMEYAMA and Y. ISHIDA, in Proceedings of the 4th International Conference on Rapidly Quenched Metals, Sendai, Japan, August 1981 edited by T. Masumoto and K. Suzuki, p. 699.
14. E. P. ELSUKOV, V. R. GALAHOV, E. E. IURTSHIKOV, S. I. NORICIN and V. S. FEBIAKINA, *Fiz. Met. Metalloved.* **52** (1981) 212.
15. Á. CZIRÁKI, in Proceedings of the Conference on Metallic Glasses, Budapest, June 1980 edited by C. Hargitai, I. Bakonyi and T. Kemény, p. II-179.
16. F. J. KEDVES, M. HORDÓS and Cs. KOPASZ, in Proceedings of the Conference on Metallic Glasses, Budapest, June 1980 edited by C. Hargitai, I. Bakonyi and T. Kemény, p. II-223.
17. K. NARITA, J. YAMASAKI and H. FUKUNAGA, *IEEE Trans. Mag. MAG*-13 (1977) 1544.
18. A. E. BERKOWITZ, J. D. LIVINGSTON, B. D. NATHAN and J. L. WALTER, *J. Appl. Phys.* **50** (1979) 1754.
19. B. ARONSSON and I. ENGSTRÖM, *Acta Chem. Scand.* **14** (1960) 1403.
20. N. F. CHABAN and Yu. B. KUZ'MA, *Inorg. Mater.* **6** (1970) 883.
21. M. HANSEN and K. ANDERKO, "Constitution of Binary Alloys" (McGraw-Hill Book Company, New York, 1958) p. 249.
22. W. KÖSTER and T. GÖDECKE, *Z. Metallkd.* **59**

(1968) 602.
23. L. HÄGGSTRÖM, L. GRANÄS, R. WÄPPLING and S. DEVANARAYANAN, *Phys. Scr.* 7 (1973) 125.
24. L. P. ANDREJEVA and P. W. GELD, *Fiz. Met. Metalloved* 19 (1965) 70.
25. U. KÖSTER and U. HEROLD, *Scripta Metall.* 12 (1978) p. 75.
26. A. INOUE, T. MASUMOTO, M. KIKUCHI and T. MINEMURA, *J. Jpn. Inst. Met.* 42 (1978) 294.
27. A. DATTA, N. J. De CRISTOFARO and L. A. DAVIS, in Proceedings of the 4th International Conference on Rapidly Quenched Metals, Sendai, Japan, August 1981 edited by T. Masumoto and K. Suzuki, p. 1007.
28. J. L. WALTER, S. F. BARTRAM and R. R. RUSSELL, *Metall. Trans. A* 9A (1978) 805.

Received 18 October
and accepted 13 December 1982